Oligomers as Triggers for Responsive Liquid Crystals

Young-Ki Kim,[†] Krishna R. Raghupathi,[‡] Joel S. Pendery,[†] Piyachai Khomein,[‡] Uma Sridhar,[‡] Juan de Pablo,[§,#,] S. Thayumanavan[‡,*], and Nicholas L. Abbott[†,*]*

[†]Department of Chemical and Biological Engineering, University of Wisconsin-Madison, 1415 Engineering Drive, Madison, WI 53706

[‡]Department of Chemistry, University of Massachusetts Amherst, 710 North Pleasant Street, Amherst, MA 01003

[§]Institute for Molecular Engineering, University of Chicago, Chicago, IL 60637, USA

[#]Argonne National Laboratory, Argonne, IL 60439, USA

*corresponding authors

ABSTRACT: We report an investigation of the influence of aqueous solutions of amphiphilic oligomers on the ordering of micrometer-thick films of thermotropic liquid crystals (LCs), thus addressing the gap in knowledge arising from previous studies of the interactions of monomeric and polymeric amphiphiles with LCs. Specifically, we synthesized amphiphilic oligomers (with decyl hydrophobic and pentaethylenegylcol hydrophilic domains) in monomer, dimer and trimer

forms, and incubated aqueous solutions of the oligomers against nematic films of 4'-pentyl-4-biphenylcarbonitrile (5CB). All amphiphilic oligomers caused sequential surface-driven orientational (planar to homeotropic) and then bulk phase transitions (nematic to isotropic) with dynamics depending strongly on degree of oligomerization. The dynamics of the orientational transitions accelerated from monomer to trimer, consistent with the effects of an increase in adsorption free energy. The mechanism underlying the orientational transition, however, involved a decrease in anchoring energy and not change in easy axis of the LC. In contrast, the rate of the phase transition induced by absorption of oligomers into the LC decreased from monomer to trimer, suggesting that constraints on configurational degrees of freedom influence the absorption free energies of the oligomers. Interestingly, the isotropic phase of 5CB nucleated at the aqueous-5CB interface, consistent with surface-induced disorder underlying the above-reported decrease in anchoring energy caused by the oligomers. Finally, we provided proof-of-concept experiments of the triggering of LCs using a trimeric amphiphile that is photocleaved by UV illumination into monomeric fragments. Overall, our results provide insight into the rational design of oligomers that can be used as triggers to create responsive LCs.

1. INTRODUCTION

Responsive materials undergo changes in structure and properties as a consequence of their interactions with their environment, including electrical and magnetic fields,[1-3] exchange of heat,[4-7] changes in pH,[7-10] UV irradiation,[11-14] and electrolyte composition.[15-16] This emerging class of materials has many potential applications, including as sensors,[9-11, 15-16] actuators,[5, 12-13] and controlled release of active chemical agents.[6-8, 14] Liquid crystals (LCs), in particular, offer substantial opportunities for the design of responsive materials due to their ability to amplify

molecular-level stimuli into the optical scale.[17-20] In this context, past studies[17-26] have reported on the interactions of monomeric and polymeric amphiphiles with aqueous interfaces of water-immiscible LC films and droplets. Both monomers[17-18, 24-26] and polymers[18-24] have been reported to adsorb to LC interfaces and trigger changes in ordering of the LCs that lead to easily quantified optical signals.

LCs are anisotropic condensed phases that possess both the mobility of a fluid and the long range order of crystalline solids.[27-28] The long range orientational order present in a nematic LC phase, where the constituent molecules align along a preferred axis called the director, gives rise to elasticity and the tendency of the LC director to assume an unperturbed, homogeneously aligned state. At the boundaries of a LC, the orientations assumed by LCs is dependent on the so-called anchoring of the LC molecules at that interface, and deviations away from the preferred orientation are energetically unfavorable. Consequently, in LC systems, the director profile is determined by a competition between the anchoring energy (WL^2) at the boundary of the LC and the elastic energy (KL) in the bulk of the LC, where W is the surface anchoring energy density, K is the Frank elastic constant of the LC, and L is a characteristic length of the LC system.[7, 27-30] As noted above, amphiphilic adsorbates can modify the anchoring of LCs at interfaces, and the elastic properties of the LCs transmit and amplify these change in LC anchoring throughout the volume of the LC that lies within ~100 μm of the interface.[17-20] Since LCs are birefringent, the optical appearance of the LCs, as observed using polarized optical microscopy, change with the director profile of the LCs.[31-32] Therefore, it is possible to infer the presence and behavior of amphiphiles at a LC/aqueous interface by observing the optical response of the LC film.[17-20]

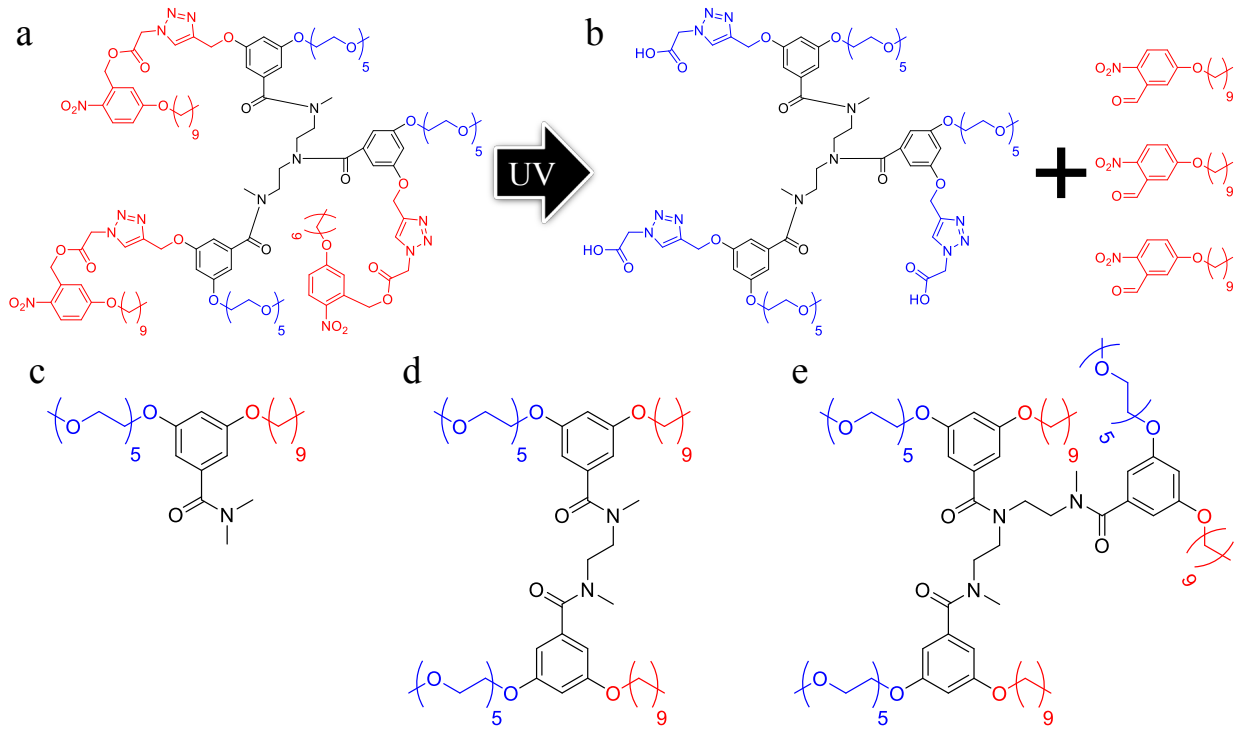

Figure 1. a,b) Molecular structure of UV-cleavable oligomer amphiphile (**UV3**) in trimer form a) before and b) after the cleavage reaction. Hydrophilic and hydrophobic groups are shown in blue and red, respectively. c-e) Molecular structures of oligomer amphiphiles with a hydrophilic polyethylene glycol functional group (shown in blue) and hydrophobic aliphatic tail (shown in red) in c) monomer (**O1**), d) dimer (**O2**), and e) trimer forms (**O3**).

The work reported in this paper is motivated by the long-term goal of designing responsive LC systems based *on stimuli-triggered changes in the degree of oligomerization of amphiphiles*. For example, Figs. 1a and 1b show the design of a trimeric amphiphile that incorporates a functional group that is cleaved upon illumination with UV light, thus converting the trimeric amphiphile (Fig. 1a, **UV3**) to three monomeric fragments and a "core" (Fig. 1b). While this strategy of UV (or chemically-triggered) disassembly of oligomers appears a promising one for the design of

responsive LC systems, a key knowledge barrier to the rationale design of such systems is the gap in understanding of how oligomeric amphiphiles interact with LCs. Whereas, as noted above, the behaviors of amphiphilic polymers and monomers have been widely studied at LC interfaces,[17-20] oligomers have not been investigated. Past studies have established, however, that the interactions of adsorbates/absorbates with nematic LCs are strongly dependent on the configurational degrees of freedom of the adsorbates/absorbates and the extent to which configurational degree of freedom are modified by the orientationally ordered environment of the LC.[9, 33-37] For example, it is well known that flexible polymers segregate from nematic LCs because the structured environment of the LC reduces the configurational degrees of freedom of the polymer chain (entropic penalty).[38-39] Accordingly, we hypothesized that the degree of oligomerization may impact the miscibility of amphiphiles with LCs and thus the response of LCs to exposure to oligomers.

Motivated by this gap in knowledge, in this paper, we report a study of the interactions of *oligomeric amphiphiles* with nematic LC films, focusing on both dynamic and equilibrium responses of the LCs, as a function of the degree of oligomerization. The molecular structures of the oligomers used in our study are shown in Figs. 1c-e. Each amphiphilic unit is composed of a hydrophobic decyl side-chain (red parts in Figs. 1c-e) and a hydrophilic pentaethylene glycol (PEG, blue parts in Figs. 1c-e) side-chain linked via an aromatic core. The monomer (**O1**), dimer (**O2**), and trimer (**O3**) are composed of the amphiphilic units, linked through a methylated amide. This amphiphile design was chosen for its facile synthesis, which allows introduction of side-chain functionalities selected to provide a response to the targeted external stimulus. In the second part of the paper, we use structure-property relationships developed in the first part of the

paper to guide the design and interpretation of experiments using the photoresponsive trimer shown in Fig. 1a.

2. METHODS

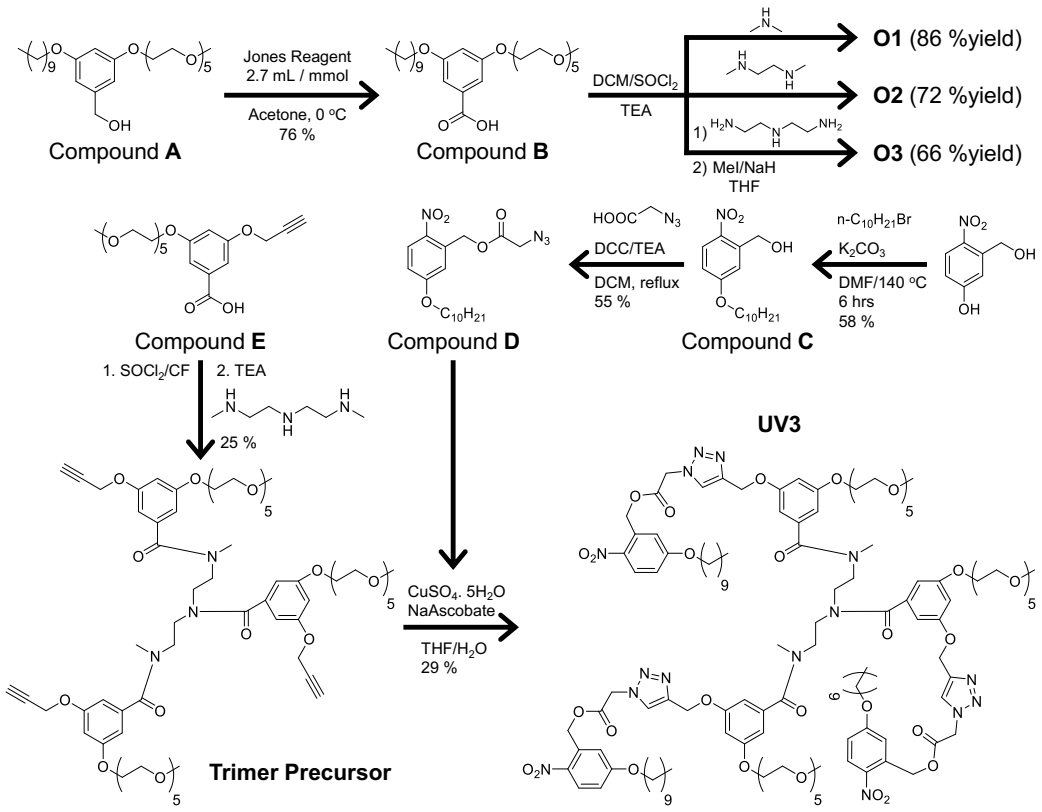

Scheme 1. Synthesis of oligomer amphiphiles.

2.1. Materials and Characterizations. All chemicals and reagents were purchased from commercial sources and were used as received, unless otherwise mentioned. ^{1}H-NMR spectra were recorded on 400 MHz Bruker NMR spectrometer using the residual proton resonance of the solvent as the internal standard. Chemical shifts are reported in parts per million (ppm). When peak multiplicities are given, the following abbreviations are used: s, singlet; d, doublet; t, triplet; m, multiplet. ^{13}C-NMR spectra were proton decoupled and measured on a 500 MHz Bruker

spectrometer with 125 MHz frequency by using carbon signal of the deuterated solvent as the internal standard. ^{1}H NMR of the methylated amphiphiles showed incorrect integrations and were rounded to the expected values. To clearly confirm the formation and purity of those products mass spectrometry was performed and reported.

2.2. Preparation of Jones Reagent. Chromium trioxide (7 g, 70 mmol) was dissolved in 10 mL of water in a 50 mL Erlenmeyer flask. The solution was then cooled using an ice bath followed by slow addition of 6.1 mL of concentrated sulfuric acid (18 M). The resultant solution was then diluted with 20 mL of water with constant stirring.

2.3. Synthesis of Acid Precursor. Compound **A** (0.77 g, 1.49 mmol) was dissolved in acetone and cooled using an ice bath. Compound **A** was synthesized following the previously reported procedure.[40-41] To this solution was added a cooled solution of Jones reagent (4 mL, 2.7 mL/mmol) drop wise, and stirred for 4 hours. Upon complete conversion of the reaction (checked by thin layer chromatography), the reaction mixture was filtered to remove a green precipitate formed. To this filtrate was added excess of isopropyl alcohol and filtered again to remove any new precipitate formed. The reaction mixture was then concentrated in vacuo and the residue was dissolved in water and the pH of this aqueous phase was adjusted to pH<3, followed by extraction with ethyl acetate (2x), the combined extracts were then dried over anhydrous Na_2SO_4. Upon evaporation of the solvent, the crude product was purified by silica gel column chromatography (using combiflash) to afford 0.6 g (76%) of compound **B**. ^{1}H-NMR (400 MHz; Acetone-d_6): δ 7.17-7.16 (m, 2H), 6.75 (t, *J* = 2.3Hz, 1H), 4.18 (t, *J* = 4.7 Hz, 2H), 4.04 (t, *J* = 6.5 Hz, 2H), 3.84 (t, *J* = 4.7 Hz, 2H), 3.68-3.54 (m, 14H), 3.47-3.45 (m, 2H), 3.28 (s, 3H), 1.82-1.75 (m, 2H), 1.53-1.45 (m, 2H), 1.41-1.28 (m, 14H), 0.88 (t, *J* = 6.9 Hz, 3H). ^{13}C-NMR (125 MHz; Acetone-d_6): δ 170.9, 167.3, 161.27, 161.09, 133.3, 108.8, 108.6, 106.8, 72.7,

71.44, 71.29, 71.25, 71.06, 70.3, 68.92, 68.75, 60.5, 58.8, 32.6, 26.7, 25.7, 23.3, 20.8, 14.50, 14.36.

2.4. General procedure for synthesis of Oligomers O1 to O3. To a solution of compound **B** in methylene chloride was added excess of thionyl chloride ($SOCl_2$) and the mixture was refluxed for 4 hours. The reaction mixture was then concentrated in vacuo to remove unreacted thionyl chloride. The crude acid chloride product was then dried for an additional 2 hours under vacuum and redispersed in methylene chloride (DCM). To this solution of acid chloride was then added appropriate equivalents of the corresponding amine (1 equivalent dimethylamine for **O1**, 0.5 equivalent N,N'-dimethyl ethylene diamine for **O2**) and triethylamine (TEA) and stirred at room temperature for 24 hours. The reaction mixture was then concentrated in vacuo and the residue was dissolved in water and extracted twice with ethyl acetate, the combined extracts were then dried over anhydrous Na_2SO_4. Upon evaporation of the solvent, the crude product was purified by silica gel column chromatography (using combiflash) to obtain oligomers **O1** and **O2** respectively. **O3** was synthesized in accordance with a previously reported procedure.[40, 42]

Monomeric Oligomer (**O1**): ^{1}H-NMR (400 MHz; $CDCl_3$): δ 6.51 (m, 2H), 6.49 (m, 1H), 4.10 (t, *J* = 4.8 Hz, 2H), 3.92 (t, *J* = 6.6 Hz, 2H), 3.84 (t, *J* = 4.8 Hz, 2H), 3.73-3.63 (m, 14H), 3.54 (dd, *J* = 5.7, 3.6 Hz, 2H), 3.37 (s, 3H), 3.08 (s, 3H), 2.96 (s, 3H), 1.75 (dt, *J* = 14.4, 7.0 Hz, 2H), 1.44-1.33 (m, 14H), 0.88 (t, *J* = 6.8 Hz, 3H). ^{13}C- NMR (125 MHz; $CDCl_3$): δ 171.4, 160.4, 159.9, 138.2, 105.8, 105.4, 102.7, 72.0, 70.92, 70.72, 70.69, 70.67, 70.62, 69.7, 68.4, 67.7, 59.1, 39.6, 35.4, 32.0, 29.68, 29.67, 29.48, 29.43, 29.28, 26.1, 22.8, 14.2. MALDI-ToF m/z 578.40 ($C_{30}H_{53}NO_8$+Na^+ requires 578.3698).

Dimeric Oligomer (**O2**): ^{1}H-NMR (400 MHz; Acetone-d_6): δ 6.53-6.38 (m, 6H), 4.15-3.55 (m, 44H), 3.46 (dd, *J* = 5.8, 3.9 Hz, 4H), 3.28 (s, 6H), 3.05 (s, 6H), 1.77-1.67 (m, 4H), 1.48-1.30

(m, 28H), 0.88 (t, J = 6.6 Hz, 6H). ^{13}C- NMR (125 MHz; Acetone-d_6): δ 171.4, 161.0, 160.8, 140.0, 106.1, 105.9, 103.1, 72.7, 71.4, 71.1, 70.2, 68.7, 68.5, 58.8, 44.8, 37.8, 23.3, 14.4. ESI-MS m/z 1131.7344 ($C_{60}H_{104}N_2O_{16}$+Na^+ requires 1131.7298).

Trimeric Oligomer (**O3**): ^{1}H-NMR (400 MHz; Acetone-d_6): δ 6.57-6.41 (m, 9H), 4.16-3.55 (m, 60H), 3.46 (t, J = 4.8 Hz, 6H), 3.28 (s, 9H), 3.06 (s, 3H), 2.66 (s, 3H), 1.79-1.65 (m, 6H), 1.33 (d, J = 75.8 Hz, 42H), 0.88-0.86 (m, 9H). ^{13}C- NMR (125 MHz; Acetone-d_6): δ 172.0, 171.6, 161.21, 161.06, 161.00, 160.94, 160.74, 139.7, 106.32, 106.24, 106.11, 105.91, 105.54, 105.43, 103.70, 103.52, 103.1, 102.9, 72.6, 71.37, 71.32, 70.28, 70.13, 68.82, 68.72, 68.58, 68.43, 58.8, 23.3, 14.4. MALDI-ToF m/z 1685.493 ($C_{90}H_{155}N_3O_{24}$+Na^+ requires 1685.0898).

2.5. Synthesis of compound C and D. 5-hydroxy-2-nitrobenzyl alcohol (500 mg, 2.96 mmol) was dissolved in DMF (10 mL). Potassium carbonate (820 mg, 5.94 mmol) and n-decyl bromide (720 mg, 3.26 mmol) were added into the solution. The reaction was stirred at 140 °C for 6 hours under argon atmosphere. The reaction was then cooled down to room temperature and 90 mL of water was added to the reaction. The product was extracted into ethyl acetate and washed with water and brine and dried over sodium sulfate. The product was further purified by flash column chromatography (hexane/ethylacetate) to give yellow liquid compound **C** (530 mg, 58%). ^{1}H-NMR ($CDCl_3$): δ 8.17 (d, 1H), 7.19 (d, 1H), 6.88 (dd, 1H), 4.98 (s, 2H), 4.07 (t, 3H), 1.82 (m, 2H), 1.46 (m, 2H), 1.40-1.20 (b, 12H), 0.88 (t, 3H).

Compound **C** (530 mg, 1.71 mmol) and 2-azido acetic acid (190 mg, 1.88 mmol) were dissolved in dichloromethane (10 mL). *N,N'*-dicyclohexyl carbodiimide (DCC, 387 mg, 1.88 mmol) was then added to the reaction followed by triethylamine (TEA, 0.26 mL, 1.88 mmol). The reaction was stirred at room temperature for 12 hours. All solid was then removed my filtration and the product was purified by flash column chromatography (hexane/ethylacetate) to

give yellow liquid compound **D** (370 mg, 55%). ^{1}H-NMR ($CDCl_3$): δ 8.21 (d, 1H), 7.03 (d, 1H), 6.91 (dd, 1H), 5.66 (s, 2H), 4.05 (t, 2H), 4.01 (s, 2H), 1.82 (m, 2H), 1.46 (m, 2H), 1.40-1.20 (b, 12H), 0.88 (t, 3H). ^{13}C-NMR ($CDCl_3$) : δ 167.8, 163.8, 140.1, 134.3, 128.4, 114.9, 113.5, 69.2, 64.7, 50.6, 32.0, 29.7, 29.4, 29.1, 26.0, 22.8, 14.2. ESI/Mass: Calc. ($C_{19}H_{28}N_4O_5$+Na^+) 415.1958 found 415.2733.

2.6. Synthesis of trimer precursor. Compound **E** (400 mg, 0.94 mmol), which was synthesized following the previously reported procedure,[42] was dissolved in chloroform (1 mL). Thionyl chloride (1 mL, 13.8 mmol) was added to the reaction and it was stirred at 60 °C for 6 hours. Solvent and the excess of $SOCl_2$ were removed under vacuum to give the acid chloride derivative. Then, it was dissolved again in chloroform (1 mL). 1,7-dimethyl ethylene triamine (26 mg, 0.20 mmol) was added followed by TEA (0.4 mL, 2.8 mmol). 1,7-dimethyl ethylene triamine was synthesized following the previously reported procedure.[43] The reaction was stirred at room temperature for 14 hours. The product was purified by flash column chromatography (dichloromethane/methanol) to yield a viscous yellow liquid (95 mg, 25%). ^{1}H-NMR ($CDCl_3$): δ 6.68-6.57 (m, 6H), 6.46-6.34 (m, 3H), 4.57 (s, 6H), 3.99 (m, 6H), 3.78 (b, 6H), 3.72-3.62 (b, 42H), 3.54 (t, 6H), 3.37 (s, 9H), 2.66 (s, 3H), 2.22 (s, 6H). ESI/Mass: Calc. ($C_{69}H_{101}N_3O_{24}$+Na^+) 1378.6673 found 1378.6738.

2.7. Synthesis of UV-cleavable trimer (UV3). Trimer precursor (95 mg, 0.07 mmol) and compound **D** (117 mg, 0.30 mmol) were dissolved in tetrahydrofuran (THF). Copper sulfate pentahydrate (75 mg, 0.30 mmol) and sodium L-ascobate (60 mg, 0.30 mmol) were added to the solution. Couple drops of water were added into the mixture. The reaction was stirred at 60 °C for 6 hours. The solid was removed by filtration and the filtrate was purified by flash column chromatography to yield a viscous yellow liquid product (51 mg, 29%). ^{1}H-NMR ($CDCl_3$): δ

8.20 (d, 3H), 7.78 (s, 3H), 6.95-6.90 (m, 6H), 6.61-6.60 (m, 3H), 6.59 (t, 3H), 6.57-6.56 (m, 3H), 5.64 (s, 6H), 5.30 (s, 6H), 5.22 (s, 6H), 4.10 (t, 6H), 4.06 (t, 6H), 3.83 (t, 6H), 3.70-3.60 (b, 50H), 3.54 (m, 6H), 3.37 (s, 9H), 3.08 (s, 6H), 1.83 (m, 6H), 1.48 (m, 6H), 1.40-1.30 (b, 36H), 0.88 (t, 9H). ESI/Mass: Calc. ($C_{126}H_{185}N_{15}O_{39}$+$Na^+$) 2555.2852 found 2555.1102.

3. RESULTS and DISCUSSION

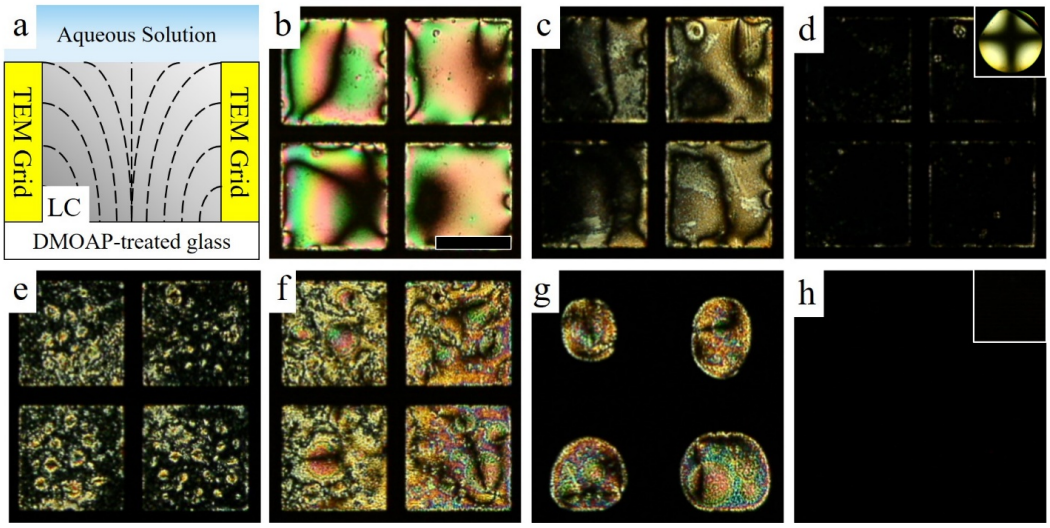

Figure 2. a, b) Schematic illustration (side view) and optical micrographs (top view, crossed polars) of 5CB films hosted in a TEM grid (10 μm in thickness) supported on a DMOAP-treated glass substrate and immersed under a PBS aqueous solution. Dashed lines in a) indicate the orientation of LC. c-h) Sequential micrographs of the LC film following addition of **O2** (C_2=0.08 mM) into the aqueous phase at c) 4, d) 5, e) 11, f) 12, g) 20, and h) 31 hours. Insets in d) and h) are the corresponding conoscopic textures. Scale bar, 200 μm.

Our initial experiments were performed to determine if amphiphilic oligomers **O1-O3** would partition to LC interfaces and influence the ordering of LCs. To this end, a LC film (10 μm in

thickness) was prepared by depositing nematic 4'-pentyl-4-biphenylcarbonitrile (5CB) into a gold TEM grid placed on a glass substrate functionalized with dimethyloctadecyl[3-(trimethoxysilyl)propyl]ammonium chloride (DMOAP). The DMOAP functionalization was performed to impose a homeotropic orientation on 5CB at the treated substrate.[44-45] Subsequently, the LC film was immersed into an aqueous bath containing 10 mM phosphate buffered saline (PBS) at pH 7.4 and the relevant amphiphilic oligomer (Fig. 2a).

We first investigated the influence of the dimeric oligomer (**O2**) dispersed in the aqueous solution on the orientation of 5CB at the LC/aqueous interface by characterizing the optical response of LC films using polarizing optical microscopy (POM).[18, 20] Each LC film, when immersed under aqueous PBS (no oligomer), exhibited a Schlieren texture with dark brushes (Fig. 2b) that correspond to regions of the LC in which the director is aligned either parallel or perpendicular to one of the crossed polarizers.[27-28, 31] Because 5CB anchors with a perpendicular orientation (homeotropic) at the DMOAP-coated glass substrate, the bright optical appearance of the LC film arises from planar anchoring of nematic 5CB at interfaces to the bulk aqueous phases with neutral pH and low ionic strength.[18, 20] These so-called hybrid boundary conditions induced a continuous bend of the director within the 5CB film (Fig. 2a). We note that the Schlieren texture also indicates that the azimuthal anchoring of the LC at the aqueous interface is degenerate (Fig. 2b). Following the introduction of 0.08 mM **O2** into the bulk aqueous phase, we made two key observations. First, we observed the brightness of the LC film to diminish (Fig. 2c), forming a dark monodomain after 5 hours (Fig. 2d, 1st transition). When observing the dark state of the LC under conoscopic observation, we found a "Maltese cross" isogyre (inset in Fig. 2d) that indicates uniform homeotropic ordering of the LC across the LC film.[4] Second, after 11 hours of incubation, bright domains emerged (Fig. 2e) and grew to cover the entire LC

film (Fig. 2f, 2nd transition). Subsequently, dark domains appeared at the edges of the birefringent LC films, forming isolated bright domains that decreased in size (Fig. 2g) until the film assumed again a uniform dark appearance (Fig. 2h, 3rd transition). The final state exhibited a dark texture (no Maltese cross) under conoscopy (inset in Fig. 2h).

The 1st transition (Figs. 2b-d) reported above (dark state with Maltese cross) reveals that **O2** within the bulk aqueous phase initially partitioned onto the LC/aqueous interface to cause an orientational transition from an initial tangential orientation to a homeotropic orientation. This type of transition in orientation can occur through at least two possible mechanisms[18-20]: (i) a change in the easy axis, i.e. the preferred orientation of the director is changed by interactions of the alkyl chains of **O2** with mesogens at the interface, or (ii) a decrease in the surface anchoring energy (WL^2) that allows the orientation of LC at the aqueous interface to relax to that imposed by the DMOAP-treated glass substrates (to minimize the elastic energy (KL)). To reveal the origin of the ordering transition, we prepared two 5CB films supported on glass substrates that were coated with either DMOAP or polyimide (PI) that was rubbed to achieve unidirectional planar alignment. The thickness of each LC film was 10 μm. This film thickness was selected to create easily quantified changes in optical retardance of LC films with an effective birefringence of $0 \leq \Delta n \leq 0.2$, where $\Delta n = 0.2$ is the birefringence of 5CB[1].

In air, the 5CB film supported on the DMOAP slide was uniformly homeotropic (Fig. 3a), consistent with past reports of homeotropic anchoring of 5CB at interfaces to air,[20, 46] whereas the 5CB film supported on the rubbed PI-coated surface exhibited a birefringent texture corresponding to a hybrid configuration arising from planar anchoring at the PI interface and homeotropic anchoring at the air interface (Fig. 3d). In aqueous PBS, because the LC/aqueous interface anchors the LC in a degenerate tangential orientation, the DMOAP-supported film

showed the Schlieren texture (Fig. 3b), as reported above. In contrast, the LC film supported on the PI-coated surface exhibited a uniform planar alignment, leading to a bright appearance without dark brushes and a coloration corresponding to higher order optical retardance (Fig. 3e) as compared to that exhibited in air. Finally, we added **O2** into the overlying aqueous phase (C_2=0.15 mM) and equilibrated the 5CB films for 4 hours. As **O2** molecules partitioned to the LC/aqueous interface, the DMOAP-supported film restored the original dark appearance (Fig. 3c). In contrast, the PI-supported film retained the bright optical texture and coloration (Fig. 3f) observed before the introduction of **O2** (Fig. 3e, uniform planar anchoring). If the adsorption of **O2** onto the LC/aqueous interface had modified the easy axis of the LC, the PI-supported film would have transformed to an optical appearance similar to the PI-supported film in air (Fig. 3d, hybrid anchoring). Our observations, therefore, suggests that the mechanism by which **O2** causes the ordering transition reported in Figs. 2b-d (1st transition) involves a decrease in the anchoring strength of the 5CB at the aqueous interface. This mechanism contrasts to past studies of conventional surfactants and phospholipids which have established that the amphiphiles cause a change in orientation of the easy axis.[18-20] A separate study has used molecular simulations to elucidate the molecular details of the interaction of **O2** with 5CB and concluded that **O2** induces disorder (local melting) of the near-surface region of the nematic 5CB at the aqueous interface. This insight is consistent with our experimental conclusion that **O2** induces a change in the anchoring energy but not easy axis of the LC.[47] We return to this point below.

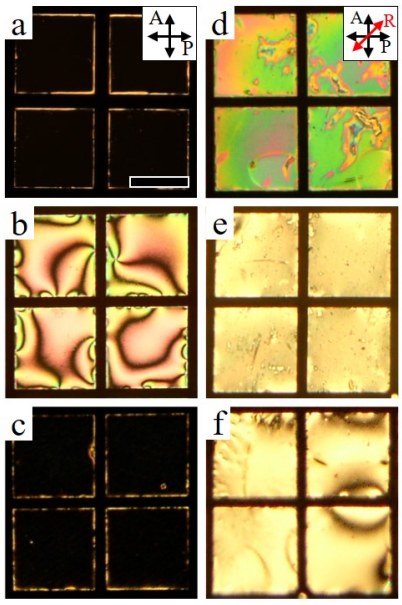

Figure 3. Optical micrographs of 5CB films supported on glass substrates coated with a-c) DMOAP and d-f) a rubbed polyimide following contact with a,d) air and aqueous solutions b,e) without and c,f) with **O2** (C_2=0.15 mM). R, P and A indicate a rubbing direction and orientation of polarizer and analyzer, respectively. Scale bar, 200 μm.

As noted above, following the 1st transition to the dark homeotropic state (Fig. 2d), the LC films immersed in aqueous **O2** exhibited a subsequent transition to a transient bright state (Figs. 2e-g) and then a second and final dark state (Fig. 2h). The final dark state (Fig. 2h) differed from the homeotropic state discussed above (Fig. 2d) in two important ways. First, whereas the edge of the LC within each grid square was bright in the first dark state (Fig. 2d; due to interaction of the LC with the vertical surfaces of the grid), no bright edges were present in the final dark state (Fig. 2h). Second, in contrast to the first dark state, as noted above, conoscopic observation of the film in the final dark state did not generate a Maltese cross (insets in Figs. 2d and 2h). These two observations suggest that the final dark state arises from either (i) the absence of the 5CB in

the grid (due to dewetting or solubilization of the LC) or (ii) the formation of an isotropic phase (I) of 5CB. Reflection mode imaging of the grid confirmed that 5CB remained in the grid (Fig. S1), and thus we concluded that the final dark state corresponded to an isotropic phase of 5CB. That is, the orientational transition that was driven by the interaction of **O2** with the aqueous interface of nematic 5CB was followed by a phase transition which transformed the nematic 5CB to an isotropic phase.

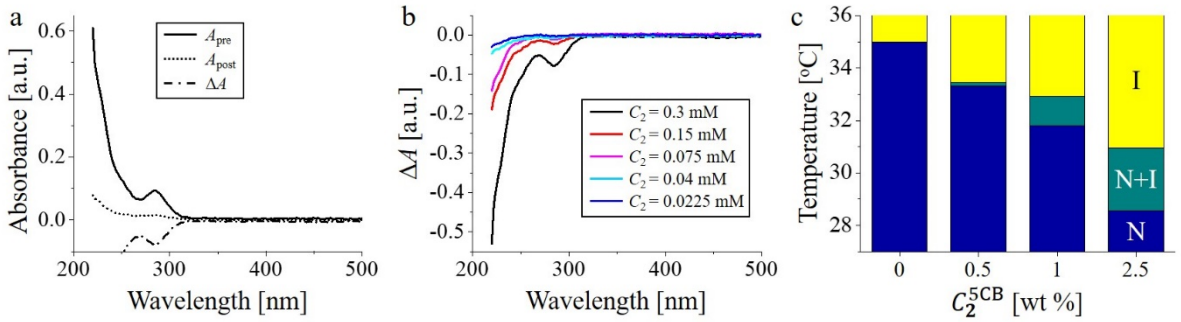

Figure 4. a) Absorbance of aqueous solutions with **O2** (initial C_2=0.3 mM) before (A_{pre}, solid line) and after incubation of a 5CB film (A_{post}, dotted line) along with its difference spectrum ($\Delta A = A_{post} - A_{pre}$, dash dot line). b) ΔA with respect to initial C_2. c) Phase diagram of 5CB as a function of the concentration of **O2** doped in 5CB (C_2^{5CB}).

To provide insight into the mechanism through which **O2** caused the 5CB film to undergo a N-to-I phase transition, we measured UV-visible absorption spectra of the aqueous **O2** solutions before (A_{pre}) and after incubation (A_{post}) against the 5CB film. For an aqueous solution with initial C_2=0.3 mM (Fig. 4a), we observed a significant decrease in absorbance following incubation against the 5CB (at λ=284 nm, absorbance of the aromatic groups of the dimer). The decrease in absorbance ($\Delta A = A_{post} - A_{pre}$) indicates partitioning of **O2** into the 5CB film. Consistent

with this interpretation, the differential absorbance ($\Delta A<0$) grew in magnitude with increase in the initial value of C_2 (Fig. 4b). From the measured change in A of an aqueous solution of **O2** (initial C_2=0.3 mM) upon incubation with a 5CB film (Fig. 4a), we calculated that the concentration of **O2** dissolved within 5CB (C_2^{5CB}) increased to 14.5 wt% (Fig. S2 and SI text). To determine the influence of **O2** on the phase behavior of 5CB, we measured a phase diagram of 5CB doped with **O2**. As shown in Fig. 4c, with increase in C_2^{5CB}, we observed a broadening of the temperature range over which coexisting N and I phases (N+I) were observed along with a decrease in a clearing temperature (N+I-to-I, T_C). By measuring the temperature at which a 5CB film incubated against 0.3 Mm **O2** underwent a I-to-N+I transition (16 °C, Fig. S3) and comparing it to the phase diagram in Fig 4c, we estimated $C_2^{5CB} \sim 13.9$ wt%, in good agreement with our independent estimate based on the decrease in A (C_2^{5CB}=14.5 wt%).

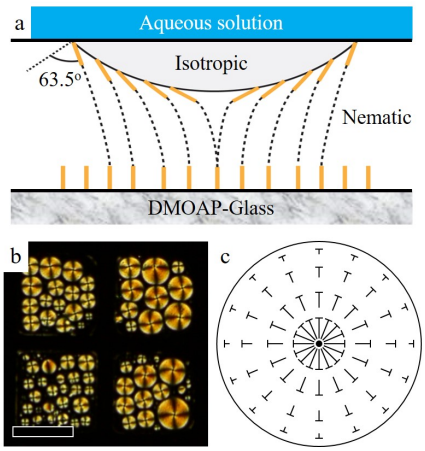

Figure 5. a) Schematic illustration (side-view) of the LC film with a director profile (dotted lines) at the transient bright state. Yellow bars and dashed lines indicate an ordering of LCs at interfaces and within the film, respectively. b) Optical micrographs (top-view, crossed polars)

and c) director profiles of bright domains in the LC film generated by isotropic domains of 5CB at the LC/aqueous interface. Scale bar, 200 μm.

Having established that the final dark state of the 5CB film contacting **O2** corresponds to an isotropic phase, we return to the observation of transient bright domains that precede this final state (Figs. 2d-f). We hypothesized that these domains arise from processes that take place during the N-to-I phase transition of the 5CB. As noted above, our experimental observations indicate that the orientational transition caused by adsorption of **O2** at the aqueous interface (Figs. 2b-d) is due to a decrease in anchoring energy, an observation that is consistent with insights from molecular dynamics simulations revealing that adsorption of **O2** causes melting of the nematic phase within a thin film located a few nanometers from the aqueous interface.[47] Guided by these observations, we hypothesized that nucleation of the isotropic phase caused by uptake of **O2** would occur at the aqueous interface of the LC film (Fig. 5a). To test this prediction, we incubated a 40 μm-thick LC film against aqueous **O2** (C_2=0.3 mM) until birefringent domains appeared in a homeotropic monodomain (Fig. 5b). By adjusting the vertical location of the focal plane of the microscope, we established that the bright domains were located near the aqueous interface (Fig. 5a). The bright domains arise from the orientational anchoring of nematic 5CB at its isotropic phase, which was measured to be θ=63.5^o from the interface normal (Figs. 5a,c).[48-49] This tilted orientation of the nematic phase is sufficient to cause the bright birefringent states.[4] We also interpret our observations to indicate that the shapes of the domains of isotropic 5CB corresponded to spherical caps (Fig. 5). The interfacial tension of the nematic/isotropic interface (σ_{NI}=1.5 ± 0.6 10^{-5} J/m^2) is approximately two orders of magnitude lower than that of the N-water (σ_{NW}) or I-water (σ_{IW}) interfacial tensions

(σ_{NW} = 7x10^{-3} J/m^2, σ_{IW} = 6x10^{-3} J/m^2 at T=35°C)[50-51] and thus $\sigma_{NW}>\sigma_{IW}>>\sigma_{NI}$. To minimize interfacial energies,[52] therefore, the isotropic domain of 5CB forms a spherical cap protruding into the nematic phase with the aqueous interface remaining largely flat (Fig. 5a). The diameter of each isotropic domain is much larger than the depth of penetration of the cap into the nematic phase, consistent with estimates of interfacial free energies (see SI). We also observed the isotropic domains of 5CB at the aqueous interface to be mobile and to merge with isotropic regions of 5CB that accumulated at the grid edges, a behavior that is also consistent with localization of the isotropic domains at the aqueous interface (not solid/LC interface). Importantly, the observation that the isotropic domains nucleated at the **O2**-decorated interface provides support for our conclusion that **O2** alters the orientation of the LC through surface-induced melting of the nematic phase.

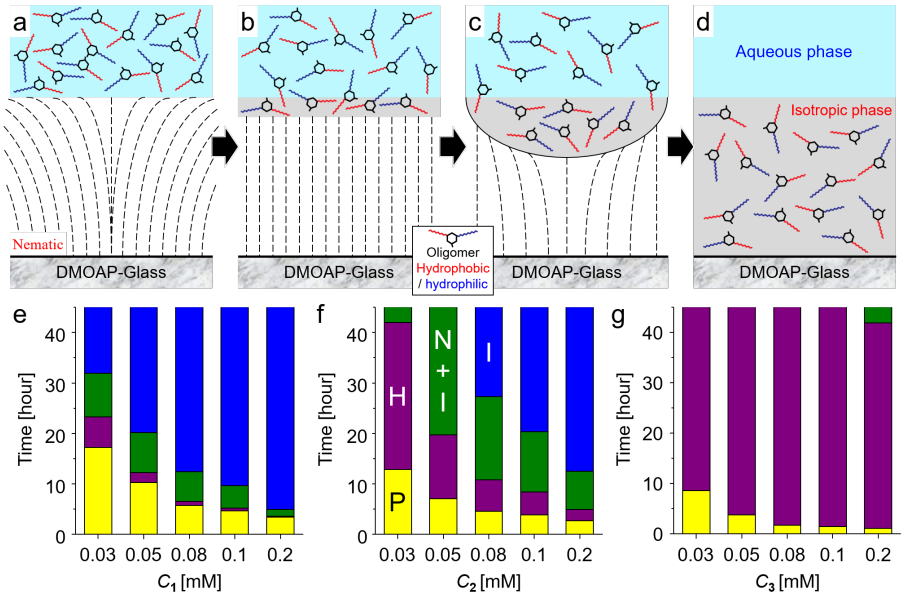

Figure 6. a-d) Schematic illustrations of LC film contacting an aqueous solution containing oligomeric amphiphiles, yielding an anchoring transition from a) a planar to b) homeotropic orientation at LC/aqueous interfaces, and then a phase transition from a nematic to c) nematic-

isotropic coexistence and ultimately to d) an isotropic phase. e-g) Time-dependent anchoring and phase transitions of the LC films in aqueous solutions with e) **O1**, f) **O2**, and g) **O3** as a function of their concentrations. P, H, N+I, and I indicate nematic films with planar (yellow bar) and homeotropic anchoring (purple bar) at the LC/aqueous interface, formation of isotropic droplets (green bar, nematic-isotropic coexistence phase), and complete transition to isotropic phase (blue bar), respectively.

Next, we sought to determine the extent to which the degree of oligomerization impacted responses of the LC films to the oligomeric amphiphiles (Figs. 6a-d). Specifically, we compared the dynamics of the transitions triggered by **O1** (monomer), **O2** (dimer), and **O3** (trimer), as a function of their initial concentration in the bulk aqueous phase (Figs. 6e-g). We make three key observations from the data in Figs. 6e-g. First, all three oligomers exhibited the same progression of orientational and phase states. The concentrations at which they were observed and their lifetimes, however, were dramatically different for each oligomer. Second, with increase in initial concentration of each oligomer in the aqueous solution, we observed the dynamics of the anchoring transition to the homeotropic state and then phase transition to N+I or I state to accelerate, indicating that the rates of uptake of the oligomers onto the LC/aqueous interfaces and then into the bulk of the LC films were concentration-dependent. Third, for a fixed concentration, with increase in degree of oligomerization, we measured the dynamics of the anchoring transition to the homeotropic orientation to accelerate. In contrast, the phase transitions from N (homeotropic anchoring)-to-N+I or N+I-to-I slowed with increase in degree of oligomerization. For example, at $C_1=C_2=C_3=0.05$ mM, we measured the transition to the homeotropic orientation to be complete at 10.2 hours for **O1**, 7.1 hours for **O2**, 3.8 hours for **O3**,

whereas the N (homeotropic state)-to-N+I phase transition occurred at 12.3 hours for **O1**, 19.7 hours for **O2**, and >60 hours for **O3**. If **O1**-**O3** are compared with the same concentrations of amphiphilic units in aqueous solutions (e.g., at C_1=0.15, C_2=0.1, C_3=0.05), however, the LC films assumed homeotropic orientations with comparable dynamics, suggesting that the ordering of LC is strongly coupled to the interactions of the amphiphilic units of the oligomers; homeotropic states were observed at 3.9 hours for C_1=0.15, 3.8 hours for C_2=0.1, and 3.8 hours for C_3=0.05. The distinct dynamics exhibited by the oligomers leads to the important conclusion that an increase in degree of oligomerization will i) accelerate the interactions of oligomers with LCs at the LC/aqueous interface that cause the homeotropic orientation and ii) suppress the absorption of oligomers into the bulk of the LC films (thus slowing the transition to the isotropic phase).

The distinct behaviors of the monomeric (**O1**), dimeric (**O2**), and trimeric (**O3**) amphiphiles, as described above, led us to hypothesize that UV-triggered cleavage of a trimeric amphiphile (**UV3**, Fig. 1a) should generate distinct changes in both equilibrium and dynamic orientational states and phase states of films of 5CB. To test this prediction, we incubated an aqueous solution of **UV3** against 5CB (C_{UV}=0.1 mM). The 5CB, which was supported on a DMOAP-coated glass substrate, initially exhibited a typical Schlieren texture (Fig. 7a). The film was observed to undergo an anchoring transition to a homeotropic orientation over 5 hours (Fig. 7b). The resultant homeotropic anchoring was maintained for several days without showing evidence of birefringent domains, similar to our observations with trimeric amphiphile **O3** (Fig. 6g). In addition, we explored the reversibility of adsorption of **UV3** at the LC/aqueous interface and compared it to **O3**. When the overlying aqueous solution of **UV3** (C_{UV}=0.1 mM) was replaced by water (C_{UV}=0 mM) following 5 hours of incubation against the LC film (Figs. 7b,c),

desorption of **UV3** occurred within 2 hours as evidenced by a transition in the optical appearance of the LC film from a dark monodomain (Fig. 7b) to a birefringent Schlieren texture (Fig. 7c). Similarly, when aqueous **O3** (C_3=0.1 mM) was replaced with water (C_3=0 mM) following incubations of DMOAP-supported LC films for 5 hours, we observed the homeotropic dark state to become birefringent, consistent with reversible adsorption, as observed with **UV3**. When combined, these results reveal that **O3** and **UV3** trigger similar changes in the LC.

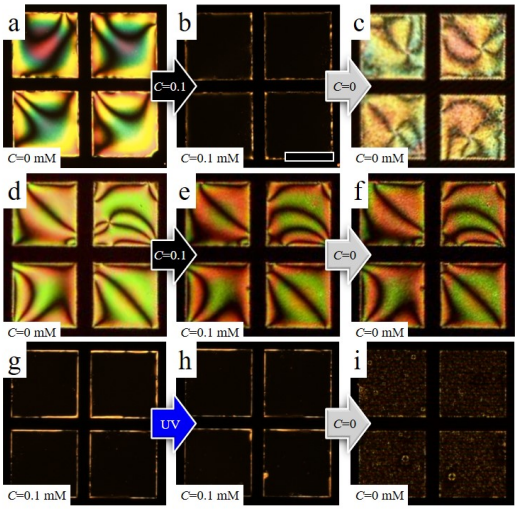

Figure 7. a-f) Optical micrographs (crossed polars) of 5CB films immersed in aqueous solutions with a-c) **UV3** (C_{UV}=0.1 mM) or d-f) cleaved **UV3** (C_{CUV}=0.1 mM) at a,d) 0 and b,e) 5 hours, and c, f) after incubation against water for 2 hours. g-i) Optical micrographs of LC films g) equilibrated in aqueous **UV3** (C_{UV}=0.1 mM) for 4 hours followed by h) 1 hour of UV irradiation and i) 2 hours incubation after dilution of **UV3** concentration to 0 mM. Scale bar, 200 μm.

Next, we explored how the UV-induced cleavage products of **UV3** influenced a film of 5CB. As shown in Figs. 1a,b, UV cleavage generates three monomeric fragments and a core unit. We irradiated an aqueous solution of **UV3** (C_{UV}=0.1 mM) with UV light (wavelength of 365 nm,

power 8 W) for an hour to cleave **UV3** into fragments. Completion of the cleavage reaction was verified by measurements of UV-visible absorbance of the aqueous **UV3** solution (Fig. S4). Following incubation of the cleaved **UV3** solution against a DMOAP-supported LC film for 5 hrs, in contrast to **UV3** prior to cleavage (Figs. 7a,b), the LC did not exhibit a dark appearance (Figs. 7d,e). This result is consistent with cleavage of **UV3** and indicates that the cleavage products of **UV3** (monomeric fragments, Fig. 1b) caused neither an anchoring transition nor phase transition in the 5CB. We note that same concentration of the monomeric amphiphile **O1** (C_1=0.3 mM) in an aqueous solution induces both anchoring and phase transitions in 5CB films over 5 hours of incubation (Fig. 6e). The structures of **O1** and the fragments of cleaved **UV3**, however, differ in important ways (Figs. 1b,c): although both possess decyl chains, the fragments of **UV3** do not possess the hydrophilic pentaethyleneglycol chains of **O1** and thus are unlikely to be as interfacially active as **O1**. This difference in structure is consistent with our observation that the fragments of **UV3** did not cause transient homeotropic states of the LC. We also speculate that the sparing water solubility of the **UV3** fragments leads to their aggregation in bulk aqueous solution such that they are kinetically trapped and unable to partition into the LC (no phase transition).

To investigate the *in situ* optical response of the LC film to UV-triggered cleavage of **UV3**, we equilibrated a 5CB film against an aqueous solution of **UV3** (C_{UV}=0.1 mM) to achieve the homeotropic LC orientation and then irradiated the system with UV light for 1 hour. Interestingly, we measured no detectable departure of the LC film from the dark homeotropic state (Figs. 7g,h). This result is surprising because, as reported above, the cleavage products of UV3 present in an aqueous solution do not impose a homeotropic orientation (Fig. 7e). We also investigated the dynamics of desorption of the **UV3** cleavage products from the aqueous

interface. A UV-exposed LC sample (decorated with **UV3**) did not show any significant change in optical appearance after equilibration for 2 hours against an aqueous solution free of **UV3** for 2 hours (Figs. 7h, i). In contrast, we observed **UV3** to desorb from LC/aqueous interface in the absence of UV irradiation within 2 hours (Figs. 7b,c). We speculate that the absence of reversible desorption of **UV3** cleavage products is due to the hydrophobic nature of the fragments (see above).

Overall, the results above indicate that the dynamics of the LC response to **UV3** is altered by UV cleavage of the trimeric amphiphile. Specifically, UV-triggered cleavage of the trimer in aqueous solution leads to strikingly different responses of the LC: **UV3** triggers a transition to homeotropic anchoring (Fig. 7b) whereas the cleavage products of **UV3** do not (Fig. 7e). In addition, UV-cleavage of the trimer adsorbed on the interface of the LC leads to distinct differences in the dynamic response of the LC to contact with water: **UV3** generates a transition from homeotropic to planar anchoring (Fig. 7c) whereas the cleavage products of **UV3** maintain the homeotropic orientation of the 5CB (Fig. 7i). In addition to revealing that oligomers form the basis of a promising class of triggers for the design of responsive LC systems, our work also hints that an understanding of the kinetics of these systems will be important challenge to address in future studies aimed at development of rational design principles.

4. CONCLUSION

In summary, we have characterized the interactions of nematic LC films with aqueous solutions of amphiphilic oligomers in monomer (**O1**), dimer (**O2**), and trimer forms (**O3**). Specifically, we found that the oligomeric amphiphiles **O1**-**O3** caused nematic 5CB to undergo sequential anchoring (planar to homeotropic) and phase transitions (nematic to isotropic) with

dynamics that dependent strongly on degree of oligomerization. The dynamics reflected the relative rates of adsorption onto the LC/aqueous interface and subsequent absorption into the LC film. Significantly, the two transitions appear fundamentally connected, as the orientational and phase transition appear to arise from amphiphile-induced melting of the nematic phase of 5CB at aqueous interface and within the bulk phase, respectively. We also explored the extent to which transformations in degree of oligomerization can be used as a trigger for LCs by exploring the properties of a UV-cleavable trimeric oligomer (**UV3**) that was cleaved into three monomeric fragments and a core unit in response to UV irradiation (λ=365 nm). We found that UV cleavage of the trimer led to striking changes in the dynamics of the response of the LCs, supporting our conclusion that molecular triggering of LCs via changes in degree of oligomerization appears a fruitful strategy for further exploration. For example, we envision future designs of oligomers that are functionalized with ligands that are targeted by specific antibodies. Because immunoglobulin G (IgG) has two binding regions, binding of oligomers to the IgG will lead to a change in the degree of oligomerization of the amphiphiles and thus changes in the dynamics of triggering of LCs. Alternatively, enzymatically catalyzed cross-linking of oligomers should lead to large changes in the dynamic and equilibrium responses of LCs. These directions of inquiry and others will rely heavily on the advances reported in this paper.

ASSOCIATED CONTENT

Supporting Information. The supporting information is available free of charge on the ACS Publications website at DOI:

Materials; Preparation of LC film; Calculation of radius and penetration depth of isotropic domain; Calculation on the amount of **O2** absorbed into a 5CB film; Optical micrograph of a

film of isotropic 5CB under reflection mode (Figure S1); Absorption of aqueous solutions with respect to C_2 (Figure S2); Phase transition of a film of isotropic 5CB incubated in an aqueous **O2** upon cooling (Figure S3), UV-visible absorbance spectra of the aqueous **UV3** upon UV irradiation (Figure S4) (PDF)

AUTHOR INFORMATION

Corresponding Author

*Email: depablo@uchicago.edu

*Email: thai@chem.umass.edu

*Email: nlabbott@wisc.edu

Notes

The authors declare no competing financial interest.

ACKNOWLEDGMENT

We acknowledge support of this research from the Army Research Office through W911NF-15-1-0568 and W911NF-17-1-0575. Additional support was provided by the National Science Foundation (CBET 1508987 and DMR-1435195). Partial support and facilities support from the Wisconsin MRSEC is also acknowledged (DMR-1121288 and DMR-1720415).

REFERENCES

1. Yang, D.-K.; Wu, S.-T., *Fundamentals of Liquid Crystal Devices*. John Wiley & Sons, Ltd.: Chichester, 2006.
2. Yeh, P.; Gu, C., *Optics of liquid crystal displays*. John Wiley & Sons, Inc.: New York, 1999.
3. Gwag, J. S.; Kim, Y. K.; Lee, C. H.; Kim, J. H., Realization of Multi-Stable Ground States in a Nematic Liquid Crystal by Surface and Electric Field Modification. *Sci. Rep.* **2015,** *5*, 11368.
4. Kim, Y.-K.; Senyuk, B.; Lavrentovich, O. D., Molecular reorientation of a nematic liquid crystal by thermal expansion. *Nat Commun* **2012,** *3*, 1133.
5. Ohm, C.; Brehmer, M.; Zentel, R., Liquid Crystalline Elastomers as Actuators and Sensors. *Adv. Mater.* **2010,** *22* (31), 3366-3387.
6. Fong, W. K.; Hanley, T.; Boyd, B. J., Stimuli responsive liquid crystals provide 'on-demand' drug delivery in vitro and in vivo. *J. Control. Release* **2009,** *135* (3), 218-226.
7. Kim, Y.-K.; Wang, X.; Mondkar, P.; Bukusoglu, E.; Abbott, N. L., Self-reporting and self-regulating responsive liquid crystals. *Nature* **2018,** *DOI: 10.1038/s41586-018-0098-y*.
8. Nazaruk, E.; Miszta, P.; Filipek, S.; Gorecka, E.; Landau, E. M.; Bilewicz, R., Lyotropic Cubic Phases for Drug Delivery: Diffusion and Sustained Release from the Mesophase Evaluated by Electrochemical Methods. *Langmuir* **2015,** *31* (46), 12753-12761.
9. Kwon, J.-Y.; Khan, M.; Park, S.-Y., pH-Responsive liquid crystal double emulsion droplets prepared using microfluidics. *RSC Adv.* **2016,** *6* (61), 55976-55983.
10. Bi, X. Y.; Hartono, D.; Yang, K. L., Real-Time Liquid Crystal pH Sensor for Monitoring Enzymatic Activities of Penicillinase. *Adv. Funct. Mater.* **2009,** *19* (23), 3760-3765.
11. Kim, Y.-K.; Huang, Y.; Tsuei, M.; Wang, X.; Gianneschi, N. C.; Abbott, N. L., Multi-Scale Responses of Liquid Crystals Triggered by Interfacial Assemblies of Cleavable Homopolymers. **2018**, 10.1002/cphc.201800106.
12. Gelebart, A. H.; Mulder, D. J.; Varga, M.; Konya, A.; Vantomme, G.; Meijer, E. W.; Selinger, R. L. B.; Broer, D. J., Making waves in a photoactive polymer film. *Nature* **2017,** *546* (7660), 632-636.
13. Yamada, M.; Kondo, M.; Mamiya, J. I.; Yu, Y. L.; Kinoshita, M.; Barrett, C. J.; Ikeda, T., Photomobile polymer materials: Towards light-driven plastic motors. *Angew. Chem.-Int. Edit.* **2008,** *47* (27), 4986-4988.
14. Barhoumi, A.; Liu, Q.; Kohane, D. S., Ultraviolet light-mediated drug delivery: Principles, applications, and challenges. *J. Control. Release* **2015,** *219*, 31-42.
15. Carlton, R. J.; Gupta, J. K.; Swift, C. L.; Abbott, N. L., Influence of Simple Electrolytes on the Orientational Ordering of Thermotropic Liquid Crystals at Aqueous Interfaces. *Langmuir* **2012,** *28*, 31-36.
16. Zou, J.; Bera, T.; Davis, A. A.; Liang, W.; Fang, J., Director Configuration Transitions of Polyelectrolyte Coated Liquid-Crystal Droplets. *J. Phys. Chem. B* **2011,** *115* (29), 8970-8974.
17. Popov, P.; Mann, E. K.; Jakli, A., Thermotropic liquid crystal films for biosensors and beyond. *J. Mat. Chem. B* **2017,** *5* (26), 5061-5078.
18. Bukusoglu, E.; Pantoja, M. B.; Mushenheim, P. C.; Wang, X.; Abbott, N. L., Design of responsive and active (soft) materials using liquid crystals. *Annual Review of Chemical and Biomolecular Engineering* **2016,** *7*, 163-196.

19. Miller, D. S.; Wang, X. G.; Abbott, N. L., Design of Functional Materials Based on Liquid Crystalline Droplets. *Chem. Mater.* **2014,** *26* (1), 496-506.
20. Carlton, R. J.; Hunter, J. T.; Miller, D. S.; Abbasi, R.; Mushenheim, P. C.; Tan, L. N.; Abbott, N. L., Chemical and biological sensing using liquid crystals. *Liq. Cryst. Rev.* **2013,** *1* (1), 29-51.
21. Sidiq, S.; Prasad, G.; Mukhopadhaya, A.; Pal, S. K., Poly(L-lysine)-Coated Liquid Crystal Droplets for Cell-Based Sensing Applications. *J. Phys. Chem. B* **2017,** *121* (16), 4247-4256.
22. Bera, T.; Deng, J.; Fang, J., Protein-Induced Configuration Transitions of Polyelectrolyte-Modified Liquid Crystal Droplets. *J. Phys. Chem. B* **2014,** *118* (18), 4970-4975.
23. Kinsinger, M. I.; Sun, B.; Abbott, N. L.; Lynn, D. M., Reversible control of ordering transitions at aqueous/liquid crystal interfaces using functional amphiphilic polymers. *Adv. Mater.* **2007,** *19* (23), 4208-4212.
24. Lockwood, N. A.; Gupta, J. K.; Abbott, N. L., Self-assembly of amphiphiles, polymers and proteins at interfaces between thermotropic liquid crystals and aqueous phases. *Surf. Sci. Rep.* **2008,** *63* (6), 255-293.
25. Alino, V. J.; Pang, J.; Yang, K. L., Liquid Crystal Droplets as a Hosting and Sensing Platform for Developing Immunoassays. *Langmuir* **2011,** *27* (19), 11784-11789.
26. Fletcher, P. D. I.; Kang, N.-G.; Paunov, V. N., UV Polymerisation of Surfactants Adsorbed at the Nematic Liquid Crystal-Water Interface Produces an Optical Response. *ChemPhysChem* **2009,** *10* (17), 3046-3053.
27. Kleman, M.; Lavrentovich, O. D., *Soft Matter Physics: An Introduction*. Springer: New York, 2003.
28. de Gennes, P. G.; Prost, J., *The Physics of Liquid Crystals*. Clarendon Press: Oxford, 1993.
29. Kim, Y.-K.; Shiyanovskii, S. V.; Lavrentovich, O. D., Morphogenesis of defects and tactoids during isotropic nematic phase transition in self assembled lyotropic chromonic liquid crystals. *J. Phys.: Condens. Matter* **2013,** *25*, 404202.
30. Wood, T. A.; Lintuvuori, J. S.; Schofield, A. B.; Marenduzzo, D.; Poon, W. C. K., A self-quenched defect glass in a colloid-nematic liquid crystal composite. *Science* **2011,** *334*, 79-83.
31. Dierking, I., *Textures of Liquid Crystals*. Wiley-VCH Verlag GmbH & Co. KGaA: New York, 2004.
32. Demus, D.; Goodby, J.; Gray, G. W.; Spiess, H.-W.; Vill, V., *Handbook of Liquid Crystals*. Wiley-VCH Verlag GmbH: New York, 1998; Vol. Vol. 2
33. Omer, M.; Khan, M.; Kim, Y. K.; Lee, J. H.; Kang, I.-K.; Park, S.-Y., Biosensor utilizing a liquid crystal/water interface functionalized with poly(4-cyanobiphenyl-4 '-oxyundecylacrylate-b-((2-dimethyl amino) ethyl methacrylate)). *Colloid Surf. B-Biointerfaces* **2014,** *121*, 400-408.
34. Kim, J.; Khan, M.; Park, S.-Y., Glucose Sensor using Liquid-Crystal Droplets Made by Microfluidics. *ACS Appl. Mater. Interfaces* **2013,** *5* (24), 13135-13139.
35. Seo, J.-M.; Khan, W.; Park, S.-Y., Protein detection using aqueous/LC interfaces decorated with a novel polyacrylic acid block liquid crystalline polymer. *Soft Matter* **2012,** *8* (1), 198-203.
36. Khan, W.; Choi, J. H.; Kim, G. M.; Park, S. Y., Microfluidic formation of pH responsive 5CB droplets decorated with PAA-b-LCP. *Lab Chip* **2011,** *11* (20), 3493-3498.

37. Lee, D.-Y.; Seo, J.-M.; Khan, W.; Kornfield, J. A.; Kurji, Z.; Park, S.-Y., pH-responsive aqueous/LC interfaces using SGLCP-b-polyacrylic acid block copolymers. *Soft Matter* **2010,** *6* (9), 1964-1970.
38. Utracki, L. A.; Jamieson, A. M., *Polymer Physics: From Suspensions to Nanocomposites and Beyond*. John Wiley & Sons, INC.: Hoboken, New Jersey, 2010.
39. Scruggs, N. R.; Kornfield, J. A., Synergistic ordering of side-group liquid crystal polymer and small molecule liquid crystal: Order and phase Behavior of nematic polymer solutions. *Macromol. Chem. Phys.* **2007,** *208* (19-20), 2242-2253.
40. Raghupathi, K. R.; Sridhar, U.; Byrne, K.; Raghupathi, K.; Thayumanavan, S., Influence of Backbone Conformational Rigidity in Temperature-Sensitive Amphiphilic Supramolecular Assemblies. *J. Am. Chem. Soc.* **2015,** *137* (16), 5308-5311.
41. Aathimanikandan, S. V.; Savariar, E. N.; Thayumanavan, S., Temperature-sensitive dendritic micelles. *J. Am. Chem. Soc.* **2005,** *127* (42), 14922-14929.
42. Wang, F.; Klaikherd, A.; Thayumanavan, S., Temperature Sensitivity Trends and Multi-Stimuli Sensitive Behavior in Amphiphilic Oligomers. *J. Am. Chem. Soc.* **2011,** *133* (34), 13496-13503.
43. Truong, T. T.; Coates, G. W.; Abruna, H. D., High power organic cathodes using thin films of electropolymerized benzidine polymers. *Chem. Commun.* **2015,** *51* (78), 14674-14677.
44. Ryzhkova, A. V.; Musevic, I., Particle size effects on nanocolloidal interactions in nematic liquid crystals. *Phys Rev E* **2013,** *87* (3), 032501.
45. Conradi, M.; Ravnik, M.; Bele, M.; Zorko, M.; Zumer, S.; Musevic, I., Janus nematic colloids. *Soft Matter* **2009,** *5* (20), 3905-3912.
46. Shah, R. R.; Abbott, N. L., Principles for measurement of chemical exposure based on recognition-driven anchoring transitions in liquid crystals. *Science* **2001,** *293* (5533), 1296-1299.
47. Ramezani-Dakhel, H.; Rahimi, M.; Pendery, J. S.; Kim, Y.-K.; Roux, B.; Abbott, N. L.; de Pablo, J. J., Amphiphile Induced Phase Transition of Liquid Crystals at Aqueous Interfaces. **2018**, Submitted.
48. Faetti, S.; Palleschi, V., Nematic-Isotropic Interface of Some Members of the Homologous Series of 4-Cyano-4'-(Normal-Alkyl)Biphenyl Liquid-Crystals. *Phys Rev A* **1984,** *30* (6), 3241-3251.
49. West, J. L.; Zhang, K.; Glushchenko, A.; Andrienko, D.; Tasinkevych, M.; Reznikov, Y., Colloidal particles at a nematic-isotropic interface: Effects of confinement. *Eur Phys J E* **2006,** *20* (2), 237-242.
50. Kim, J.-W.; Kim, H.; Lee, M.; Magda, J. J., Interfacial tension of a nematic liquid crystal/water interface with homeotropic surface alignment. *Langmuir* **2004,** *20*, 8110-8113.
51. Faetti, S.; Palleschi, V., Measurements of the interfacial tension between nematic and isotropic phase of some cyanobiphenyls. *J Chem Phys* **1984,** *81* (12), 6254-6258.
52. Israelachvili, J. N., *Intermolecular and Surface Forces*. 3rd edn ed.; Elsevier Science: Burlington, 2010.

For table of Contents Only